# Nanoscale

Accepted Manuscript


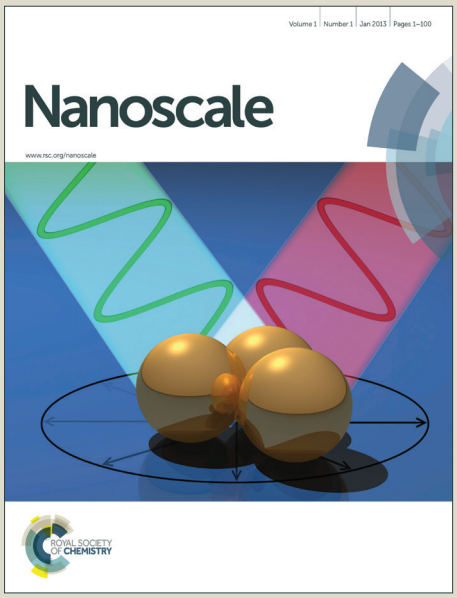

Journal Name Nanoscale Dynamic Article Links ►

Cite this: DOI:

www.rsc.org/xxxxxx

ARTICLE TYPE

# Current transport in graphene/AlGaN/GaN vertical heterostructures probed at nanoscale

**Gabriele Fisichella,[a,b] Giuseppe Greco,[a] Fabrizio Roccaforte,[a] Filippo Giannazzo *[a]**

***Received (in XXX, XXX) Xth XXXXXXXXX 20XX, Accepted Xth XXXXXXXXX 20XX***

**DOI:**

Vertical heterostructures combining two or more graphene (Gr) layers separated by ultra-thin insulating or semiconductor barriers represent very promising systems for next generation electronics devices, due to the combination of high speed operation with wide-range current modulation by a gate bias. They are based on the specific mechanisms of current transport between two-dimensional-electron-gases (2DEGs) in close proximity. In this context, vertical devices formed by Gr and semiconductor heterostructures hosting an "ordinary" 2DEG can be also very interesting. In this work, we investigated the vertical current transport in Gr/$Al_{0.25}Ga_{0.75}N$/GaN heterostructures, where Gr is separated from a high density 2DEG by a ~24 nm thick AlGaN barrier layer. The current transport from Gr to the buried 2DEG was characterized at nanoscale using conductive atomic force microscopy (CAFM) and scanning capacitance microscopy (SCM). From these analyses, performed both on Gr/AlGaN/GaN and on AlGaN/GaN reference samples using AFM tips with different metal coatings, the Gr/AlGaN Schottky barrier height $\Phi_B$ and its lateral uniformity were evaluated, as well as the variation of the carrier densities of graphene ($n_{gr}$) and AlGaN/GaN 2DEG ($n_s$) as a function of the applied bias. A low Schottky barrier (~0.40 eV) with excellent spatial uniformity was found at Gr/AlGaN interface, i.e., lower compared to the measured values for metal/AlGaN contacts, which range from 0.6 to 1.1 eV depending on the metal workfunction. The electrical behaviour of Gr/AlGaN contact has been explained by Gr interaction with AlGaN donor-like surface states located in close proximity, which are also responsible of high n-type Gr doping (~$1.3\times10^{13}$ $cm^{-2}$). An effective modulation of $n_s$ by the Gr Schottky contact was demonstrated by capacitance analysis under reverse bias. From this basic understanding of transport properties in Gr/AlGaN/GaN heterostructures, novel vertical field effect transistor concepts with high operating speed and $I_{on}/I_{off}$ ratio can be envisaged.

## 1. Introduction

Graphene[1] attracted huge scientific interests, due to the unique combination of excellent electrical[2], optical[3], thermal[4] and mechanical properties[5], paving the way to many interesting applications in ultra-fast electronics, optoelectronics, photovoltaics, devices thermal management. However, graphene suffers from an intrinsic limitation as channel material in conventional field effect transistor (FET) architectures, i.e., the low ratio between the on- and off-state currents ($I_{on}/I_{off}$), ultimately depending on the lack of a bandgap. Under this point of view, novel graphene-based hybrid devices have been proposed in the last few years, that are able to overcome this limitation. They mainly consist of vertical heterostructures combining graphene with semiconductors or ultra-thin insulating materials, including gate modulated graphene/semiconductor Schottky barrier transistors[6], silicon hot electron transistors with a graphene base[7], field-effect tunneling transistors based on graphene heterostructures with atomically thin barrier layers (such as boron nitride, molybdenum disulfide or tungsten disulphide)[8,9]. An efficient current modulation by electric field was proved in these device structures, with reported $I_{on}/I_{off}$ ratios from $10^4$ to $10^6$. Their working principles rely on some peculiar properties of graphene, such as the electronic density of states linearly depending on energy and the one-atomic-layer thickness, as well as on the specific mechanisms of current transport through the graphene/dielectric or graphene/semiconductor barriers. Such mechanisms strongly depend on the nanoscale structural and electrical properties of the interfaces, so that appropriate high resolution characterization methods are needed for their investigation.

Vertical heterostructures made with two or more graphene layers separated by thin insulating materials[8,9] received particular interest, also because of the electronic correlation effects that can be observed due to the Coulombian interaction between 2DEGs of Dirac Fermions in close proximity[10,11]. In this context, vertical devices formed by graphene and semiconductor heterostructures hosting a high mobility "ordinary" 2DEG deserve also attention, since they can represent the basis a new class of Dirac-Schrödinger hybrid electron systems, as recently discussed in the literature in the case of graphene/AlGaAs/GaAs heterostructures

[12,13]. Among the possible semiconductors that can be considered for such hybrid systems with graphene, $Al_xGa_{1-x}N$/GaN heterostrucures[14] deserve a special interest, due to some peculiar properties (such as the wide bandgap and high critical electric field of GaN and AlGaN alloys, as well as the high mobility of the 2DEG), and to their importance in technological applications, especially in the high electron mobility transistors (HEMTs) technology[15]. Some of the peculiar properties of the AlGaN/GaN system can have a strong impact in the interaction with graphene. As an example, contrary to AlGaAs/GaAs, where a doping of the layers is typically required for the 2DEG formation, the 2DEG at the heterojunction between a strained AlGaN layer and GaN forms even in the case of unintentional doping of the semiconductors. The carriers for 2DEG formation are supplied by donor surface states of AlGaN and driven to the heterojunction by the built-in electric fields originating from the difference in the spontaneous and piezoelectric polarization between the barrier layer and GaN [16,17].

To date, some studies on graphene contacts on GaN have been reported in the literature [18], with potential applications as transparent conductive electrodes in optoelectronic devices [19], whereas only few investigations have been reported on the graphene/AlGaN/GaN system (from now on, briefly indicated as Gr/AlGaN/GaN). Graphene has been proposed as heat spreader for thermal management in high power AlGaN/GaN transistors[20], and, more recently ohmic contact formation between metal and AlGaN/GaN heterostructure via graphene insertion has been reported [21]. However, the mechanisms of current transport at Gr/AlGaN/GaN interface, and the phenomena related to the interaction of graphene and semiconductor 2DEGs have not been addressed to date.

In this paper we investigated the vertical current transport in Gr/$Al_{0.25}Ga_{0.75}N$/GaN heterostructures, where graphene is separated from a high density 2DEG by a ~24 nm thick AlGaN barrier layer. The vertical current transport from graphene to the buried 2DEG was characterized at nanoscale using current measurements by conductive atomic force microscopy (CAFM)[22] and capacitance measurements by scanning capacitance microscopy (SCM) [23]. From these analyses, performed both on graphene-coated and bare AlGaN/GaN regions using different AFM tips metal coatings, the graphene/AlGaN barrier height was extracted, as well as the variation of the carrier densities of graphene and AlGaN/GaN 2DEG as a function of the gate bias.

## 2. Results and Discussion

AlGaN/GaN heterostructures grown on Si(111) wafers by MOCVD were used in this study. The surface morphology and the structural quality of these heterostructures were preliminarily characterized by atomic force microscopy (AFM) and cross sectional Transmission Electron Microscopy (TEM). Fig.1(a) shows a typical tapping mode topographic image of the AlGaN surface. Furthermore, cross-sectional TEM images of the AlGaN/GaN heterostructure in the bright field and in the high-resolution modes are reported in Fig.1(b) and (c), respectively. The very low surface roughness (RMS=0.81 nm) compared to the typically reported values on AlGaN, and the absence of peculiar defects (dislocations or V-defects) [24] in the barrier layer demonstrate the high quality of the heterostructure. An average AlGaN/GaN 2DEG concentration ~$5\times10^{12}$ $cm^{-2}$ was measured by macroscopic capacitance-voltage measurements on large area (in the order of 1 $cm^2$) using a mercury probe equipment, while the sheet resistance (~620 Ω/sq) was evaluated on van der Pauw structures.

Single layer graphene grown by chemical vapour deposition on Cu foils was separated from Cu using electrochemical delamination [25] and transfer-printed to the AlGaN surface (see Supporting information). After graphene transfer onto AlGaN, optical microscopy inspection revealed a very poor contrast between graphene-coated and bare AlGaN regions. To characterize the quality of transferred graphene, AFM was used in combination with micro-Raman measurements. The surface morphology of graphene on AlGaN (reported Fig1(d)) showed an homogeneous crack-free material, indicating a good adhesion between graphene and AlGaN during transfer. The higher surface roughness (RMS≈1.50 nm) compared to the value on bare AlGaN is due to peculiar corrugations (wrinkles) in the monolayer graphene membrane, typically formed during graphene growth on Cu in the cool-down step [26]. Raman spectra of graphene on AlGaN (reported in Fig.1(e)) shows the characteristic G peak (at ~1592 $cm^{-1}$) and 2D peak (at ~2687 $cm^{-1}$ with FWHM≈33 $cm^{-1}$) and a low intensity D peak (at ~1350 $cm^{-1}$), indicating a negligible density of defects.

Fig.2 (a) and (b) report two different series of I-V curves collected using an Au coated AFM tip displaced on a square array of 25 positions (spaced by 1 μm each other ) on bare AlGaN (a) and graphene-coated AlGaN (b), respectively. Schematic representations of the experimental setup for local current-voltage measurements by CAFM on AlGaN/GaN and Gr/AlGaN/GaN, respectively, are also depicted in the inserts of the same figures. Both series of curves exhibit a rectifying behavior, with a negligible current at negative biases and rapidly increasing current at forward bias higher than an onset voltage. Interestingly, while a broad I-V curves distribution has been found in the case of the Au tip/AlGaN contact, a very narrow spread between curves at different positions is found for the Au tip/Gr/AlGaN contact. Furthermore, in the latter case the current onset occurs at significantly lower bias than for Au tip/AlGaN, indicating a reduced Schottky barrier height. The spread between the local I-V curves measured on bare AlGaN can be associated to surface potential fluctuations, which are typical sources of the laterally inhomogeneous Schottky barrier between metals and GaN or its alloys[27]. Differently than classical metal electrodes, consisting of polycrystalline films composed by grains with different sizes and crystalline orientations, the graphene membrane works as an uniform and atomically thin electrode which covers the AlGaN surface in a very conformal way. Most probably, the graphene electrode has an averaging effect of the AlGaN surface potential fluctuations over the typical length scale of the graphene electron mean free path $l_{gr}$, which is in the order of ~0.1μm for substrate supported graphene[28]. Clearly, $l_{gr}$ is much larger than the electron mean free path of classical metal electrodes. This averaging effect results in the observed superior uniformity of graphene Schottky contacts on the AlGaN surface.

Current transport from graphene to the AlGaN/GaN 2DEG occurs through the unintentionally doped AlGaN barrier layer. For the ~24 nm thick and defects-free barrier layer used in this

experiment, we have found that thermoionic emission is the most appropriate model to describe charge transport across this barrier, whereas tunneling phenomena can be dominant for graphene contacts to a locally thinner AlGaN layer.

The characteristic parameters of the Schottky contacts, i.e., the barrier height and the ideality factor, were extracted from the forward bias characteristics, by fitting the ln(I) vs V curves using the thermoionic emission theory. A representative ln(I)-V curve from the measured array on bare AlGaN is reported in Fig.2(c). As discussed in Ref. [29], the forward bias I-V curves of Schottky contacts on AlGaN/GaN heterostructures cannot be satisfactorily described by a single metal/AlGaN Schottky diode, rather an equivalent circuit of two diodes back-to-back in series should be used [30], as schematically illustrated in Fig.2(e), where the left diode (diode 1) represents the Schottky contact between the metal and the AlGaN barrier layer and the right diode (diode 2) represents the effective Schottky contact between the 2DEG and AlGaN. For forward polarization of the heterostructure, diode 1 and diode 2 are forward and reverse biased, respectively. Hence, according to the thermoionic emission model, the I-V curve of diode 1 can be expressed as:

$$I \approx I_{s1} \exp\left(\frac{qV_1}{n_1 kT}\right) \tag{1}$$

where

$$I_{s1} = SA^* T^2 \exp\left(-\frac{q\Phi_{B1}}{kT}\right) \tag{1a}$$

is the saturation current of diode 1, being S the tip contact area, A* the Richardson constant, k the Boltzmann constant, T the temperature, q the electron charge, $V_1$ the voltage drop across the diode 1, $n_1$ and $\Phi_{B1}$ the ideality factor and barrier height. The current voltage characteristics of the reverse biased diode 2 can be expressed as:

$$I \approx SA^* T^2 \exp\left(-\frac{q\Phi_{B2}(V_2)}{kT}\right) \tag{2}$$

where $\Phi_{B2}$ is the 2DEG/AlGaN effective barrier height, which is a function of the voltage drop $V_2$ across diode 2. Furthermore, the applied bias V is related to $V_1$ and $|V_2|$ as $V=V_1+|V_2|+IR$, where *R* is the series resistance of the circuit, whose contribution starts to dominate at high currents.

For low $V_2$ values, $\Phi_{B2}(V_2)$ can be expanded by the Taylor series and approximated to the first-order correction, as

$$\Phi_{B2}(V_2) \approx \Phi_{B2}(0) - \left[\frac{\partial \Phi_{B2}}{\partial V_2}\right]_{V_2=0} |V_2| ,$$

where $\Phi_{B2}(0)$ is the 2DEG/AlGaN barrier height at zero bias ($|V_2|=0$). This assumption is justified for low voltages across diode 2, whereas for large $|V_2|$ values, the series resistance becomes the dominant factor. Using this approximation, the reverse current across diode 2 can be expressed as:

$$I \approx I_{s2} \exp\left(\frac{q|V_2|}{n_2 kT}\right) , \tag{3}$$

with

$$I_{s2} \approx SA^* T^2 \exp\left(-\frac{q\Phi_{B2}(0)}{kT}\right) . \tag{3a}$$

Noteworthy, Eq. (3) is formally similar to the expression of forward current across diode 1. Here

$$n_2 = 1 \Big/ \left[\frac{\partial \Phi_{B2}}{\partial V_2}\right]_{V_2=0}$$

represents the effective ideality factor of diode 2, which reflects the degree of barrier height $\Phi_{B2}$ change due to the change of voltage across it, with the larger $n_2$ the smaller the change of barrier height is. According to the above arguments, the current through the heterostructure can be described as due to two diodes in series with the equivalent circuit elements as shown in Fig.2(e).

The parameters $I_{s1}$, $I_{s2}$, $n_1$, $n_2$ of the metal/AlGaN/GaN heterostructure can be extracted from the plot of ln(I) versus V in Fig.2(c), using the following procedure. Since $V \approx V_1$ in the low current regime, $I_{s1}$ and $n_1$ can be obtained by linear fitting of the ln(I)-V plot at low voltages. The intercept of the fitted straight line gives $I_{s1}$ and the slope gives the information for $n_1$. To obtain $I_{s2}$ and $n_2$, another linear fit is carried out in the higher current regime. This fit is made in the second linear region of the ln(I)-V plot at intermediate voltages, whose behavior is determined by the barrier $\Phi_{B2}$, as shown in Fig.2(c). This line was extrapolated to intercept the previous line at the intercept voltage $V_2$', assumed as the turn on voltage of the second diode with a saturation current $I_{s2}$, as indicated in the Fig.2(c). The ideality factor $n_2$ can be obtained from the slope of this linear fit. It is worth noting that the product SA* in Eqs. 1(a) and 3(a) is not exactly known, since the experimental values of Richardson constant are typically lower than the ideal one ($A^* \approx 35.8$ A/K$^2$cm$^2$) [29] and the tip contact area S can be subjected to small variations from point to point. The following procedure has been adopted to determine $\Phi_{B1}$ and $\Phi_{B2}(0)$ from the fit values of $\ln(I_{s1})$ and $\ln(I_{s2})$, without using $SA^*$. According to the band structure in Fig.2(e), the built-in potential across the AlGaN barrier layer at zero bias ($V_{tip}=0$) is:

$$\Delta V(0) = \Phi_{B1} - \Phi_{B2}(0) = \frac{kT}{q}\left[\ln(I_{s2}) - \ln(I_{s1})\right] , \tag{4}$$

where the last part of the equation derives from the difference of Eqs.1(a) and 3(a), and $\ln(I_{s2})$ and $\ln(I_{s1})$ are directly obtained from the two linear fits. $\Delta V(0)$ is also related to the difference between the positive surface polarization charge $+\sigma$ and the density $n_{s0}$ of the AlGaN/GaN 2DEG at zero bias, i.e. $\Delta V(0)=q(\sigma-n_{s0})/C_{AlGaN}$, being $C_{AlGaN}=\varepsilon_0\varepsilon_{AlGaN}/d$ the barrier layer capacitance per unit area, with d=24 nm the barrier layer thickness and $\varepsilon_{AlGaN}$= 9.375 the relative dielectric permittivity for an $Al_xGa_{1-x}N$ alloy with an Al concentration of 25% [31]. Using the $\Delta V(0)$ value obtained from the fit results (Eq. (4)) and the $\sigma$ value from macroscopic C-V mercury probe analyses ($\sigma=6.93\times10^{12}$cm$^{-2}$), the value of $n_{s0}$ can be obtained. The Fermi level position (at zero bias) with respect to the GaN conduction band minimum ($E_{cmin}$) can be expressed as a function of $n_{s0}$ as [31]

$$E_{Fs0} - E_{c\,min} = \frac{\pi\hbar^2}{q m_{eff}} n_{s0} + \frac{1}{q}\left(\frac{9\pi\hbar q^2}{8\varepsilon_0 \varepsilon_{AlGaN}\sqrt{8m_w^*}}\right)^{\frac{2}{3}} n_{s0_{100}}^{\frac{2}{3}} \tag{5}$$

being ħ the reduced Planck's constant and $m_{eff}$ the 2DEG effective mass ($m_{eff}$=0.22$m_e$).

Finally, according to the band structure in Fig.2(e), the diode 2 barrier height is $\Phi_{B2}(0)=\Delta E_c-(E_{FS0}-E_{cmin})$, being $\Delta E_C$=0.34 eV the $Al_{0.25}Ga_{0.75}N$/GaN conduction band offset. Finally, the diode 1 barrier height $\Phi_{B1}$ can be obtained using Eq. (4).

By using the above described procedure, the following local barrier height values $\Phi_{B1}$=0.96±0.33 eV, $\Phi_{B2}(0)$=0.11±0.02 eV, $n_1$=3.5±0.1, $n_2$=12.1±0.3 have been determined by fitting of the representative I-V curve in Fig.2(c). Furthermore, the local carrier density of the AlGaN/GaN 2DEG was calculated as $n_{s0}=(5.2\pm0.7)\times10^{12}$ $cm^{-2}$. Repeating the same procedure for all the local I-V curves in the array of Fig.2(a), the distributions of barrier height values and 2DEG carrier densities reported in the histograms of Fig.3(a) and (b) are obtained. The average $\Phi_{B1}$ and $\Phi_{B2}(0)$ values over the set of curves are $\Phi_{B1}$=0.95±0.12 eV and $\Phi_{B2}(0)$=0.111±0.008 eV, whereas the average $n_{s0}$ value is $n_{so}=(5.17\pm0.24)\times10^{12}$ $cm^{-2}$.

An analogous procedure has been followed to extract the characteristic electrical parameters for the Au tip/Gr/AlGaN/GaN system. By fitting the representative forward bias I-V curve in Fig.2(d) with the two diodes model in Fig.2(f), the following barrier height and ideality factor values have been obtained: $\Phi_{B1}$=0.41±0.04 eV, $\Phi_{B2}(0)$=0.077±0.002 eV, $n_1$=5.22±0.08, $n_2$=9.9±0.2. Furthermore a 2DEG density $n_{s0}=(6.22\pm0.08)\times10^{12}$ $cm^{-2}$ at the AlGaN/GaN interface was evaluated.

The histograms of the $\Phi_{B1}$, $\Phi_{B2}(0)$ and $n_{s0}$ obtained by fitting of the entire set of I-V curves on the Gr/AlGAN/GaN sample are also reported in Fig. 3(a) and (b). Interestingly, a significant reduction of the Schottky barrier height between the tip and AlGaN is found in the presence of the graphene interlayer. Furthermore, an increase of the local carrier density of the AlGaN/GaN 2DEG was also found. Noteworthy, the distribution of the barrier height values measured at different tip positions (with 1 μm spacing each other) is extremely narrow in the presence of graphene, indicating a much higher degree of spatial homogeneity of the Schottky barrier to AlGaN.

Forward I-V characterizations have been carried out on AlGaN/GaN and Gr/AlGaN/GaN heterostructures using AFM tips covered by metals with different workfunctions $W_M$. Besides gold ($W_{Au}$=5.54 eV), also platinum ($W_{Pt}$=6.13 eV), nichel ($W_{Ni}$=5.47 eV) and copper ($W_{Cu}$=5.22 eV) coatings were used [32]. The behaviour of $\Phi_{B1,}$ $\Phi_{B2}(0)$ and $n_{s0}$ vs the metal workfunction are reported in Fig.4(a) and (b), respectively, with the error bars coming from the standard deviations of measured values at different tip positions. $\Phi_{B2}(0)$ and $n_{s0}$ were found to be independent of the tip metal coating both on AlGaN/GaN and on Gr/AlGaN/GaN, with smaller values of $\Phi_{B2}(0)$ in the latter case, consistently with the larger values of $n_{s0}$. For all tip metal coatings, the $\Phi_{B1}$ values measured onto bare AlGaN are much higher than on Gr/AlGaN. Interestingly, while $\Phi_{B1}$ significantly increases as a function of $W_M$ in the case of the tip/AlGaN contact, it is almost independent on $W_M$ for the tip/Gr/AlGaN contacts.

According to the Schottky-Mott (SM) model of metal/semiconductor Schottky contacts [33,34], the expected barrier height for an ideal rectifying contact should be given by the difference between the metal workfunction $W_M$ and the semiconductor electron affinity ($\chi_{AlGaN}$≈2.7 in the case of the $Al_{0.25}Ga_{0.75}N$ alloy). However, this condition is rarely obtained in the reality, since the Schottky barrier formation depends also on the surface states of the semiconductor, that can cause a Fermi level pinning at the interface with the metal (Bardeen model [35]). In the presence of a very high surface states density, a barrier height value independent on the metal workfunction can be found. In most of the cases, an intermediate behavior between these two extremes is observed, with $\Phi_B$ increasing as a function of $W_M$ following approximately a linear trend but with a slope $S=d\Phi_B/dW_M<1$ (interface index). This is what is observed in the case of the tip/AlGaN barrier $\Phi_{B1}$ in our experiment, with S≈0.84±0.26.

Due to the different graphene doping levels by charge transfer from various metals [32], different workfunctions of graphene under the tip could be expected using different tip coatings[36]. This would imply a dependence of the tip/Gr/AlGaN barrier height on the metal tip workfunction, assuming that the contact follows the SM rule. Indeed, graphene contacts on several bulk semiconductors, such us Si, 4H-SiC, GaAs and GaN, have been found to approximately obey the SM rule [19], whereas no specific studies have been carried out for graphene on semiconductor heterostructures (i.e., in the presence of an underlying buried 2DEG). Noteworthy, the experimentally found $\Phi_{B1}$ trend independent of $W_M$ (see Fig.4(a)) suggests that the behavior of the Gr/AlGaN contact is dominated by surface states of the AlGaN. In the case of the Gr/AlGaN/GaN heterostructure, these states are located in close proximity to the graphene and are able to efficiently exchange charge with graphene. The very low Gr/AlGaN Schottky barrier, compared to the value $W_G-\chi_{AlGaN}$≈1.8 eV expected in the case of an ideal graphene contact (with $W_G$≈4.5eV for intrinsic graphene), indicates a high n-type doping of graphene, consistently the donor like character of AlGaN surface states.

According to the Bardeen model of Schottky barriers with high interface states density [35], the graphene/AlGaN Schottky contact can be described assuming the presence a very thin insulating layer (vacuum) with thickness *t* between graphene and AlGaN (see Fig.5), which can be considered completely transparent to electron transport, but able to withstand a potential drop Δ across it. The presence of an ultrathin vacuum layer between graphene and AlGaN is reasonable, considering the van der Waals bonding between the two surfaces. The positively charged AlGaN surface states are located on one side of this insulating layer, while the graphene 2DEG with electron density $n_{gr}$ is located on the other side. According to the Gauss' law the potential drop Δ must be related to $n_{gr}$ as

$$\Delta=qn_{gr}t/\varepsilon_0. \quad (6)$$

According to the band diagram in Fig.5 and using the thickness t≈0.41 nm extimated by AFM measurements of the separation between graphene and AlGaN (as discussed in the Supporting Information), the graphene density $n_{gr0}$ (at zero bias) can be obtained solving the equation:

$$\Phi_{B1}=W_G-(E_{Fgr0}-E_D)-\Delta-\chi_{AlGaN} \quad (7)$$

where $E_{Fgr0}-E_D$ is the distance between the Fermi level in graphene and the Dirac point:

$$E_{Fgr0} - E_D = \frac{\mathrm{sign}(n_{gr0})\hbar v_F \sqrt{\pi n_{gr0}}}{q}$$

with $v_F$ the graphene 2DEG Fermi velocity. This latter relation derives from the linear dispersion of energy with respect to momentum in graphene. By solving Eq.(7) the carrier density $n_{gr0}$ has been evaluated and a high n-type doping of graphene was found. As an example, $n_{gr0}=(1.29\pm0.16)\times10^{13}$ cm$^{-2}$ was obtained from the analysis of the representative I–V curve in Fig.2(d) for the Au tip/Gr/AlGaN/GaN, while the distribution of $n_{gr0}$ values at different tip positions is reported in the histogram of Fig.3(c). The theoretical Fermi velocity $v_F=1\times10^6$m/s for ideal, i.e. defects-free, graphene was used in these calculations. We also estimated that a possible local reduction of $v_F$ due to the presence of defects in the probed graphene area [37] results in a slight increase of $n_{gr0}$, which is inside the experimental error.

Up to this point, we have extracted the barrier height and the carrier densities of the 2DEG at zero bias by fitting of the forward I-$V_{tip}$ characteristics and extrapolation to $V_{tip}$=0. In the following, local capacitance-voltage measurements under reverse bias made using scanning capacitance microscopy will be used to determine the dependence of the $n_s$ and $n_{gr}$ on the applied bias. Fig.6(a) reports a schematic representation of the SCM experimental setup (see insert) and two representative C-V curves (with C the capacitance per unit area) measured on the AlGaN/GaN and on the Gr/AlGaN/GaN heterostructures using an Au coated tip.

At $V_{tip}$=0 capacitance values of ~0.31 μF/cm$^2$ and ~0.35 μF/cm$^2$ were measured on AlGaN/GaN and Gr/AlGaN/GaN, respectively. Both curves exhibit almost constant (for AlGaN/GaN) or slightly decreasing (for Gr/AlGaN/GaN) capacitance starting from $V_{tip}$=0 up to a certain negative bias and, therefore, a rapid decrease to very low capacitance values (~0.1 nF/cm$^2$) for bias $|V_{tip}|>|V_{th}|$, defined as the threshold voltage.

For $|V_{tip}|<|V_{th}|$, i.e. up to AlGaN/GaN 2DEG depletion, the capacitance of the AlGaN/GaN system can be described as the series combination of two contributions: (i) $C_{AlGaN,}$ i.e. the capacitance of the plane capacitor with the metal tip and the 2DEG as electrodes; (ii) $C_{Q,ord}$ the quantum capacitance of the AlGaN/GaN "ordinary" 2DEG [38]. The latter term is expressed as $C_{Q,ord}=m_{eff}q^2/(\pi\hbar^2)$ [39], with $m_{eff}=0.22m_e$ the electron effective mass in the $Al_xGa_{1-x}N$/GaN quantum well, and is in the order of 14.7 μF/cm$^2$, i.e., almost 50 times larger than the measured capacitance at $V_{tip}$=0. Hence, it can be concluded that its weight in the series combination is almost negligible, and the first term ($C_{AlGaN}$) gives rise to the higher capacitance level in the C-V curve for $|V_{tip}|<|V_{th}|$. For $|V_{tip}|>|V_{th}|$, i.e. under full depletion of the 2DEG, the AlGaN/GaN behaves as a single unintentionally doped semiconductor layer with large thickness, giving rise to a very low capacitance level.

In the case of the Gr/AlGaN/GaN heterostructure, an additional capacitance term, i.e., the graphene quantum capacitance $C_{Qgr}$ [40,23] should be added to the series combination of the first two terms. $C_{Qgr}$ depends on the electron energy and resembles the linear behavior of the density of states D with $|E_{Fgr}-E_D|$. As discussed more in detail in the Supporting Information section, also this quantum capacitance term is much higher than $C_{AlGaN}$ and, therefore, can be neglected in the series combination.

From the previous discussion results that, both for the AlGaN/GaN and the Gr/AlGaN/GaN heterostructures, the C-$V_{tip}$ curves are related to the 2DEG density $n_s$ at AlGaN/GaN interface [16]. Hence, the $n_s$ dependence on $V_{tip}$ can be obtained by integration of these curves [31], i.e. :

$$n_s(V_{tip}) = \frac{\int_0^{V_{tip}} C(V)dV}{q} \quad . \qquad (8)$$

Fig.6(b) reports the $n_s$-$V_{tip}$ curves obtained by integration of the representative C-$V_{tip}$ curves of Fig.6(a). Both curves exhibit a linear decrease of $n_s$ vs $|V_{tip}|$ till $n_s\approx0$. A simple way to determine the threshold voltages for the two heterostructures is fitting the linear region and taking the intercept with the $n_s$=0 baseline. A higher $V_{th}$ value is obtained in the case of the Gr/AlGaN/GaN heterostructure ($V_{th}$=-3.11 V) than in the case of the AlGaN/GaN heterostructure ($V_{th}$=-2.69 V), consistently with the higher values of $n_{s0}$.

Clearly, in the case of a biased Gr/AlGaN/GaN heterostructure, due to the electrostatic coupling between the 2DEGs in close proximity, the changes of $n_s$ in the AlGaN/GaN quantum well due to the applied bias induce also variations of the carrier density $n_{gr}$ in graphene. The behavior of $n_{gr}$ as a function of the applied bias $V_{tip}$ can be evaluated by application of the Gauss' law (as discussed in the Supporting Information) and can be expressed as:

$$n_{gr}(V_{tip}) = n_{gr0} + n_{s0} - n_s(V_{tip}) \quad . \qquad (9)$$

This is illustrated in Fig.6(c), showing an almost linear increase of $n_{gr}$ with $|V_{tip}|$ up to a saturation value ~$1.9\times10^{13}$cm$^{-2}$ for $|V_{tip}|\approx|V_{th}|$. Clearly, the initial increase of $n_{gr}$ follows the decrease of $n_s$, whereas the constant $n_{gr}$ for $|V_{tip}|>|V_{th}|$ is related to the low capacitance value of the AlGaN/GaN system after full 2DEG depletion. The relation between $n_s$ and $n_{gr}$ is reported in the insert of Fig.6(c), demonstrating a ~100× decrease of $n_s$ corresponding to a 1.5× increase of $n_{gr}$.

## 3. Conclusion

In conclusion, the physical properties of the Gr/AlGaN/GaN heterostructure have been investigated at nanoscale, demonstrating a low barrier height ($\Phi_{B1}$~0.4 eV) Gr/AlGaN Schottky contact with excellent lateral uniformity. This low barrier height value is related to the high n-type doping (~$1.3\times10^{13}$ cm$^{-2}$) of graphene in contact with AlGaN, due to the charge transfer from the donor-like surface states at AlGaN surface. Furthermore, a very efficient modulation of the AlGaN/GaN 2DEG by modulation of the Fermi level ($E_F$-$E_D$) in the graphene electrode was demonstrated. The peculiar properties of the Gr/AlGaN/GaN heterostructure, combined with the partial transparency of graphene to electric fields [8], can be exploited in the demonstration of novel device concepts, such as a vertical field effect transistor based on the control of $n_{gr}$ and $n_s$ (and, consequently, of the barrier heights $\Phi_{B1}$ and $\Phi_{B2}$) by a gate electrode, which is expected to ensure high performances in terms of $I_{on}/I_{off}$ ratio and operation speed.

## 4. Experimental Section

**Heterostructure fabrication.** $Al_{0.25}Ga_{0.75}N$/GaN heterostructures were grown by metal organic chemical vapour deposition

(MOCVD) on Si (111) wafers. Graphene was grown by Chemical Vapour Deposition on a ~25 μm thick polycrystalline copper foil at a temperature of 1000 °C by using $CH_4/H_2$ as precursors. Afterwards graphene/copper samples were coated by Poly(methyl methacrylate) (PMMA) by spin coating for 60 seconds at 1000 rounds per minutes and baked at 150°C for 10 minutes. Electrochemical delamination of graphene from copper foil was performed in a 0.2 M KOH water solution with an applied voltage of 5 V between the copper foil, used like cathode, and an anode of gold. Graphene sustained by PMMA was printed on the target substrate and PMMA was removed in Acetone at room temperature.

**TEM characterization.** The structural quality of the AlGaN/GaN heterostructure before graphene transfer was preliminarily characterized by Transmission Electron Microscopy (TEM) using a JEOL JEM 2010F equipment with a Schottky field emission gun operating at an acceleration voltage of 200 kV. Analyses were performed on cross-sectioned samples both in the bright field and in the high resolution modes.

**AFM analyses.** Tapping mode AFM measurements were carried out with Veeco DI3100 atomic force microscope with Nanoscope V controller. Commercial silicon probes with spring constant k= 20 to 80 N/m and oscillation frequency from 332 to 375 kHz mode were employed.

**Micro-Raman analyses.** Micro-Raman measurements on graphene layers onto AlGaN were carried out using a ~532 nm laser source and 100× objective magnification (~1μm lateral resolution).

**Macroscopic electrical characterization.** The average AlGaN/GaN 2DEG concentration (~$5\times10^{12}$ $cm^{-2}$) on large area (in the order of 1 $cm^2$) was measured by macroscopic capacitance-voltage measurements using a mercury probe equipment, while the heterostructure sheet resistance (~620 Ω/sq) was measured on van der Pauw structures. The average sheet resistance of graphene was also evaluated as ~1.1 kΩ/sq, using transmission line model (TLM) test patterns.

**Nanoscale electrical characterization.** Local current and capacitance measurements were carried out at room temperature by conductive atomic force microscopy (CAFM) and scanning capacitance microscopy (SCM), respectively, using a DI3100 AFM with Nanoscope V electronics. These nanoscale resolutions electrical analyses were performed both on graphene-coated and bare AlGaN regions (reference) using AFM tips with different metal coatings (i.e., Au, Pt, Cu, Ni) obtained by thin films sputtering. The force between tip and sample was properly set in order to have a stable electrical contact. In the case of CAFM analyses, during the scan a DC bias was applied between the tip and a large-area contact on bare AlGaN, and the current flowing between these two contacts was collected by a high sensitivity current amplifier in series. Clearly, the major contribution to the measured resistance is due to the vertical current path from the tip to the AlGaN/GaN 2DEG, whereas the path from this 2DEG to the large-area contact adds a series resistance contribution. In the case of SCM, in addition to the DC bias, a small amplitude modulating signal at high frequency (100 kHz) was applied to the large area contact and the capacitance variation in response to this signal was measured by a high sensitivity capacitance sensor [41,42].

## Acknowledgements

The authors acknowledge S. Di Franco (CNR-IMM) for the expert support in samples and device structures preparation and C. Bongiorno (CNR-IMM) for TEM analyses. S. Agnello from University of Palermo is acknowledged for micro-Raman analyses and useful discussions. We thank S. Ravesi from STMicroelectronics for the very interesting discussions on these experiments. N. Spartà, S. Lo Verso, C. Tringali and S. Di Marco from STMicroelectronics are acknowledged for the collaboration in the graphene transfer experiments. This work was partially supported by the national project PON Ambition Power (PON01_00700).

## Notes and references

[a] *CNR-IMM, Strada VIII, 5 - 95121 Catania, Italy.*
**Corresponding author E-mail:* ***filippo.giannazzo@imm.cnr.it***
[b] *Department of Electronic Engineering, University of Catania, Italy*

† Electronic Supplementary Information (ESI) available: Graphene transfer; Determination of graphene/AlGaN separation by AFM; Graphene carrier density in a biased Gr/AlGaN/GaN heterostructure; Quantum capacitance contributions to the capacitance-voltage characteristics of Gr/AlGaN/GaN heterostructures. See DOI:

[1] Geim, A. K.; Novoselov, K. S. The rise of graphene. *Nat. Mater.* **2007,** 6, 183.

[2] Bolotin, K.I.; Sikes, K.J.; Jiang, Z.; Klima, M.; Fudenberg, G.; Hone, J.; Kim, P.; Stormer, H.L. Ultrahigh electron mobility in suspended graphene. *Solid State Communications* **2008**, 146, 351–355.

[3] Bonaccorso, F.; Sun, Z.; Hasan, T.; Ferrari, A. C. *Graphene photonics and optoelectronics*. *Nature Photonics* **2010**, 4, 611-622.

[4] Balandin, A.; Ghosh, S.; Bao, W.; Calizo, I.; Teweldebrahn, D.; Miao, F.; Lau, C. N. Superior Thermal Conductivity of Single-Layer Graphene. *Nano Lett.* **2008**, 8, 902.

[5] Lee, C.; Wei, X.; Kysar, J. W.; Hone, J. Measurement of the Elastic Properties and Intrinsic Strength of Monolayer Graphene. *Science* **2008**, 321, 385.

[6] Yang, H.; Heo, J.; Park, S.; Song, H. J.; Seo, D. H.; Byun, K.-E.; Kim, P.; Yoo, I.; Chung, H.-J.; Kim, K. Graphene Barristor, a Triode Device with a Gate-Controlled Schottky Barrier. *Science* **2012**, 336, 1140-1142.

[7] Vaziri, S.; Lupina, G.; Henkel, C.; Smith, A. D.; Ostling, M.; Dabrowski, J.; Lippert, G.; Mehr, W.; Lemme, M. C. A Graphene-Based Hot Electron Transistor. *NanoLett.* **2013**, 13, 1435−1439

[8] Britnell, L.; Gorbachev, R. V.; Jalil, R.; Belle, B. D.; Schedin, F.; Mishchenko, A.; Georgiou, T.; Katsnelson, M. I.; Eaves, L.; Morozov, S. V.; Peres, N. M. R.; Leist, J.; Geim, A. K.; Novoselov, K. S.; Ponomarenko, L. A. Field-Effect Tunneling Transistor Based on Vertical Graphene Heterostructures. *Science* **2012**, 335, 947-950.

[9] Georgiou, T.; Jalil, R.; Belle, B. D.; Britnell, L.; Gorbachev, R. V.; Morozov, S. V.; Kim, Y.-J.; Gholinia, A.; Haigh, S. J.; Makarovsky, O.; Eaves, L.; Ponomarenko, L. A.; Geim, A. K.; Novoselov, K.S.; Mishchenko, A. Vertical field-effect transistor based on graphene–WS2 heterostructures for

flexible and transparent electronics. *Nature Nanotechnology* **2013**, 8, 100-103.

[10] Kim, S.; Jo, I.; Nah, J.; Yao, Z.; Banerjee, S. K.; Tutuc, E. Coulomb drag of massless fermions in graphene. *Phys. Rev. B* **2011**, 83, 161401(R).

[11] Gorbachev, R. V.; Geim, A. K.; Katsnelson, M. I.; Novoselov, K. S.; Tudorovskiy, T.; Grigorieva, I. V.; MacDonald, A. H.; Morozov, S. V.; Watanabe, K.; Taniguchi, T.; Ponomarenko, L. A. Strong Coulomb drag and broken symmetry in double-layer graphene**.** *Nature Physics* **2012**, 8, 896–901.

[12] Principi, A.; Carrega, M.; Asgari, R.; Pellegrini, V.; Polini, M. Plasmons and Coulomb drag in Dirac-Schrodinger hybrid electron systems. *Phys. Rev* B **2012**, 86, 085421.

[13] Gamucci, A.; Spirito, D.; Carrega, M.; Karmakar, B.; Lombardo, A.; Bruna, M.; Ferrari, A.C.; Pfeiffer, L.N.; West, K.W.; Polini, M.; Pellegrini, V. Electron-hole pairing in graphene-GaAs heterostructures, arXiv:1401.0902v1 [cond-mat.mes-hall] 5 Jan 2014

[14] M. Asif Khan, J. M. Van Hove, J. N. Kuznia, D. T. Olson, High electron mobility GaN/AlxGa1−xN heterostructures grown by low-pressure metalorganic chemical vapor deposition. *Appl. Phys. Lett.* **1991**, 58, 2408.

[15] Mishra U.K.; Parikh, P.; Wu, Y.-F. AlGaN/GaN HEMTs: An Overview of Device Operation and Applications, *Proceedings of the IEEE* **2002**, 90, 1022-1031.

[16] Ambacher, O.; Foutz, B.; Smart, J.; Shealy, J. R.; Weimann, N. G.; Chu, K.; Murphy, M.; Sierakowski, A. J.; Schaff, W. J.; Eastman, L. F.; Dimitrov, R.; Mitchell, A.; Stutzmann, M. Two dimensional electron gases induced by spontaneous and piezoelectric polarization in undoped and doped AlGaN/GaN heterostructures, *J. Appl. Phys.* **2000**, 87, 334.

[17] Ibbetson, J. P.; Fini, P. T.; Ness, K. D.; DenBaars, S. P.; Speck, J. S.; Mishra, U. K. Polarization effects, surface states, and the source of electrons in AlGaN/GaN heterostructure field effect transistors, *Appl. Phys. Lett.* **2000**, 77, 250.

[18] Chandramohan, S.; Kang, J. H.; Ryu, B. D.; Yang, J. H.; Kim, S.; Kim, H.; Park, J. B.; Kim, T. Y.; Cho, B.J.; Suh, E.-K.; Hong, C.-H. Impact of Interlayer Processing Conditions on the Performance of GaN Light-Emitting Diode with Specific NiOx/Graphene Electrode, *ACS Appl. Mater. Interfaces* **2013**, 5, 958−964.

[19] Tongay, S.; Lemaitre, M.; Miao, X.; Gila, B.; Appleton, B. R.; Hebard, A. F. Rectification at Graphene-Semiconductor Interfaces: Zero-Gap Semiconductor-Based Diodes, *Phys. Rev. X* **2012**, 2, 011002.

[20] Yan, Z.; Liu, G.; Khan, J. M.; Balandin, A. A. Graphene quilts for thermal management of high-power GaN transistors, *Nature Communications*, 3:827 | DOI: 10.1038/ncomms1828.

[21] Park, P. S.; Reddy, K. M.; Nath, D. N.; Yang, Z.; Padture, N. P.; Rajan, S. Ohmic contact formation between metal and AlGaN/GaN heterostructure via graphene insertion, *Appl. Phys. Lett.* **2013**, 102, 153501.

[22] Sonde, S.; Giannazzo, F.; Raineri, V.; Yakimova, R.; Huntzinger, J.-R.; Tiberj, A.; Camassel, J. Electrical properties of the graphene/4H-SiC (0001) interface probed by scanning current spectroscopy, Phys. Rev. B **2009**, 80, 241406(R).

[23] Giannazzo, F.; Sonde, S.; Raineri, V.; Rimini, E. Screening Length and Quantum Capacitance in Graphene by Scanning Probe Microscopy. *Nano Lett.* **2009**, 9, 23.

[24] Greco, G.; Fiorenza, P.; Giannazzo, F.; Alberti, A.; Roccaforte, F. Nanoscale electrical and structural modification induced by rapid thermal oxidation of AlGaN/GaN heterostructures, *Nanotechnology* **2014**, 25, 025201.

[25] Wang, Y.; Zheng, Y.; Xu, X.; Dubuisson, E.; Bao, Q.; Lu, J.; Loh, K. P. Electrochemical Delamination of CVD Grown Graphene Film: Toward the Recyclable Use of Copper Catalyst, *ACS Nano*, **2011**, 5, 9927–9933.

[26] Zhang, Y.; Gao, T.; Gao, Y.; Xie, S.; Ji, Q.; Yan, K.; Peng, H.; Liu, Z. Defect-like structures of graphene on copper foils for strain relief investigated by high-resolution scanning tunneling microscopy, *ACS Nano* **2011**, 5, 4014-4022.

[27] Iucolano, F.; Roccaforte, F.; Giannazzo, F.; Raineri, V. Barrier inhomogeneity and electrical properties of Pt/GaN Schottky contacts, *J. Appl. Phys.* **2007**, 102, 113701.

[28] Giannazzo, F.; Sonde, S.; Lo Nigro, R.; Rimini**,** E.; Raineri, V. Mapping the Density of Scattering Centers Limiting the Electron Mean Free Path in Graphene, *Nano Lett.* **2011**, 11, 4612–4618.

[29] Lv, Y.; Lin, Z.; Corrigan, T. D.; Zhao, J.; Cao, Z.; Meng, L.; Luan, C.; Wang, Z.; Chen, H. Extraction of AlGaN/GaN heterostructure Schottky diode barrier heights from forward current voltage characteristics. *J. Appl. Phys.* **2011**, 109, 074512.

[30] Chen, C. H.; Baier, S. M.; Arch, D. K.; Shur, M. S. A new and simple model for GaAs heterojunction FET gate characteristics, *IEEE Trans. Electron Devices* **1988**, 35, 570.

[31] Ambacher, O.; Smart, J.; Shealy, J. R.; Weimann, N. G.; Chu, K.; Murphy, M.; Schaff, W. J.; Eastman, L. F.; Dimitrov, R.; Wittmer, L.; Stutzmann, M.; Rieger, W.; Hilsenbeck, J.; *J. Appl. Phys.* **1999**, 85, 3222.

[32] Giovannetti, G.; Khomyakov, P. A.; Brocks, G.; Karpan, V. M.; van den Brink, J.; Kelly, P. J.; Doping Graphene with Metal Contacts, *Phys. Rev. Lett.* **2008**, 101**,** 026803.

[33] Schottky, W.; Theory of blocking layer and point rectifiers, *Zeit. f. Phys.* **1939**, 113**,** pp. 367-414.

[34] Mott, N. F.; Note on the Contact between a Metal and an Insulator or Semiconductor, *Proc. Cambr. Philos. Soc.*3, 4, 568 (1938).

[35] Bardeen, J.; Surface states and rectification at a metal semiconductor contact. *Phys. Rev.* **1947**, 71, 717-727.

[36] Song, S. M.; Park, J. K.; Sul, O. J.; Cho, B. J.; Determination of Work Function of Graphene under a Metal Electrode and Its Role in Contact Resistance, *Nano Lett.* **2012**, 12, 3887−3892.

[37] Tapasztó, L.; Dobrik, G.; Nemes-Incze, P.; Vertesy, G.; Lambin, Ph.; Biró, L. P.; Tuning the electronic structure of graphene by ion irradiation, *Phys. Rev B* **78**, 233407 (2008).

[38] Park, P. S.; Nath, D. N.; Rajan, S.; Quantum Capacitance in N-Polar GaN/AlGaN/GaN Heterostructures. *IEEE Electron Device Letters* **2012**, 33, 991-993.
[39] Luryi, S.; Quantum capacitance devices, *Appl. Phys. Lett.* **1988**, 52, 501-503.
[40] Xia, J.; Chen, F.; Li, J.; Tao, N. Measurement of the quantum capacitance of graphene. *Nature Nanotechnology* **2009**, 4, 505-509.
[41] Giannazzo, F.; Fiorenza, P.; Raineri, V. Carrier transport in advanced semiconductor materials, *Applied Scanning Probe Methods* **2008**, Vol. 8-10, Edited by B. Bhushan, H. Fuchs and M. Tomitori, Springer-Verlag, Heidelberg.
[42] Giannazzo, F.; Raineri, V.; Rimini, E. Transport properties of graphene with nanoscale lateral resolution*, Scanning Probe Microscopy in Nanoscience and Nanotechnology 2*, **2011**, Edited by B. Bhushan,, Springer-Verlag Berlin Heidelberg.



 

Cite this: DOI:
www.rsc.org/xxxxxx

**ARTICLE TYPE**

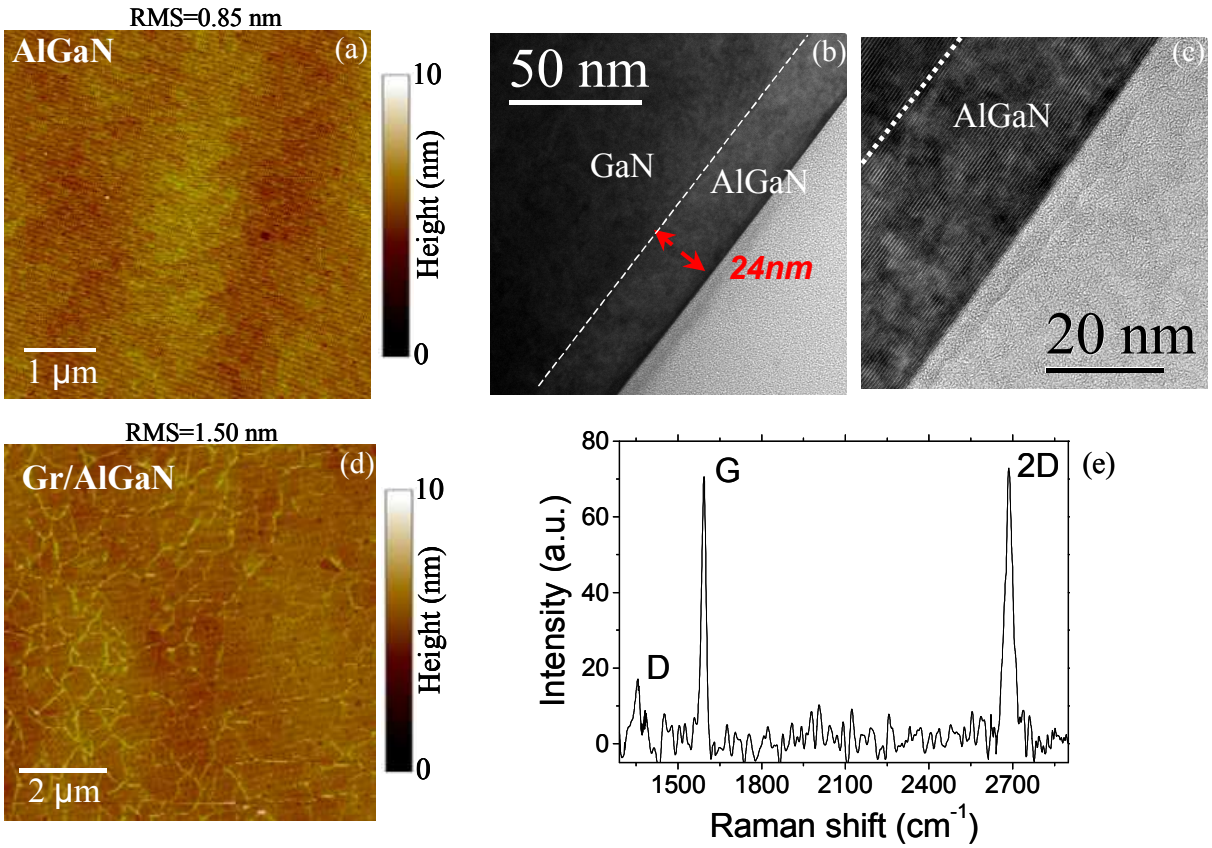


**Fig.1.** AFM morphology (a) and cross-sectional TEM image in bright field (b) and at high-resolution (b) of the AlGaN/GaN heterostructure before graphene transfer. AFM morphology of graphene on AlGaN (c). Raman spectra of graphene on AlGaN (c) showing the characteristic G (~1592 $cm^{-1}$) and 2D (~2687 $cm^{-1}$) peak and a very low intensity D peak (~1350 $cm^{-1}$), indicating a low density of defects.

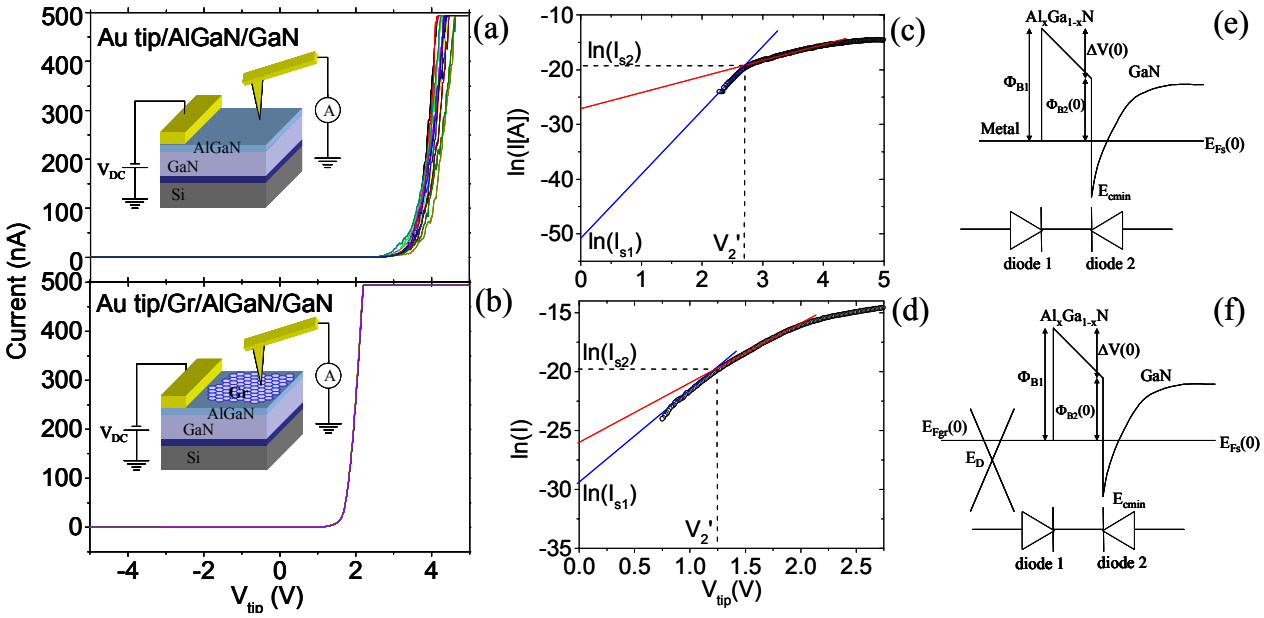


**Fig. 2.** Two different series of I-V curves collected using an Au coated AFM tip displaced on a square array of 25 positions on AlGaN/GaN (a) and Gr/AlGaN/GaN (b). Schematic representations of the experimental setup for local current-voltage measurements by CAFM in the inserts of (a) and (b). Fitting of two representative forward bias ln(I)-V curves acquired on AlGaN (c) and Gr/AlGaN (d). Conduction band diagrams of AlGaN/GaN (e) and Gr/AlGaN/GaN heterostructures (f) with the equivalent circuit of a Schottky AlGaN/GaN diode represented as two diodes back-to-back in series.

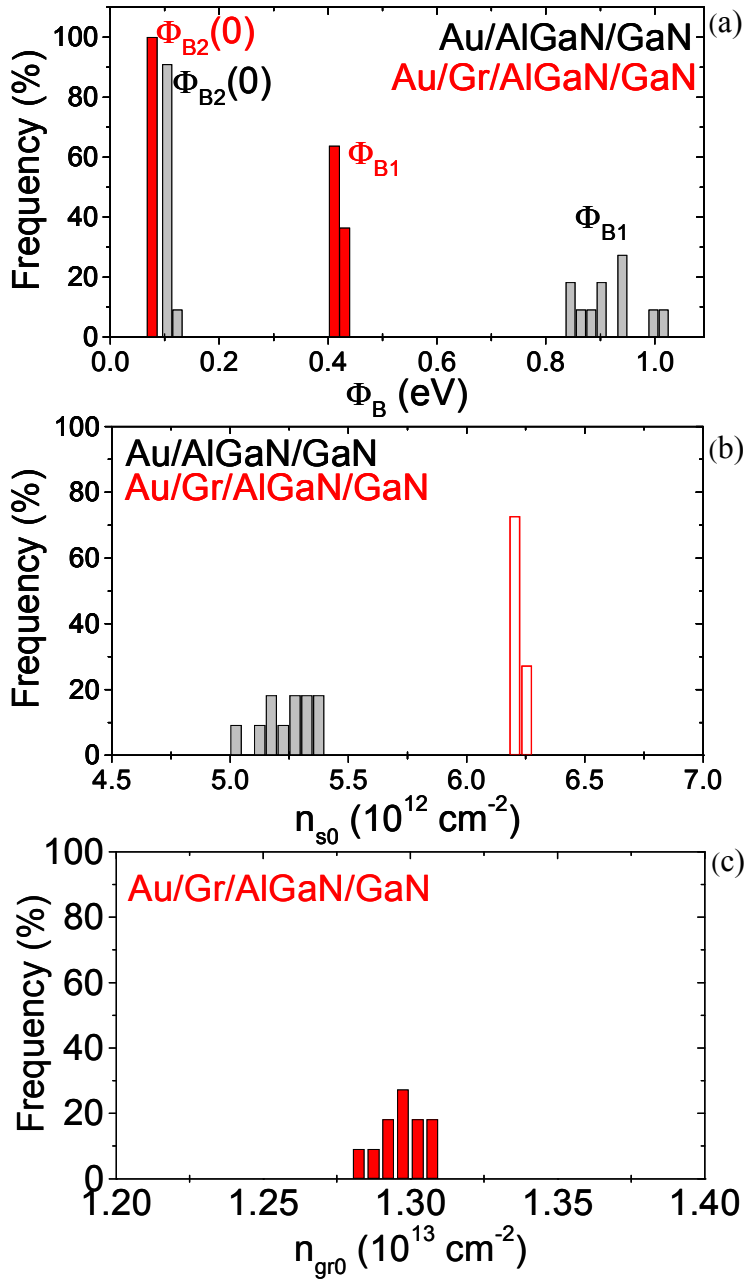


**Fig.3.** Histograms of the $\Phi_{B1}$, $\Phi_{B2}(0)$ (a), and $n_{s0}$ (b) obtained on an array of 25 tip positions (spaced by 1 μm each other) on the AlGaN/GaN and Gr/AlGAN/GaN heterostructures. Histogram of $n_{gr0}$ at the different positions in the Gr/AlGAN/GaN heterostructure (c).

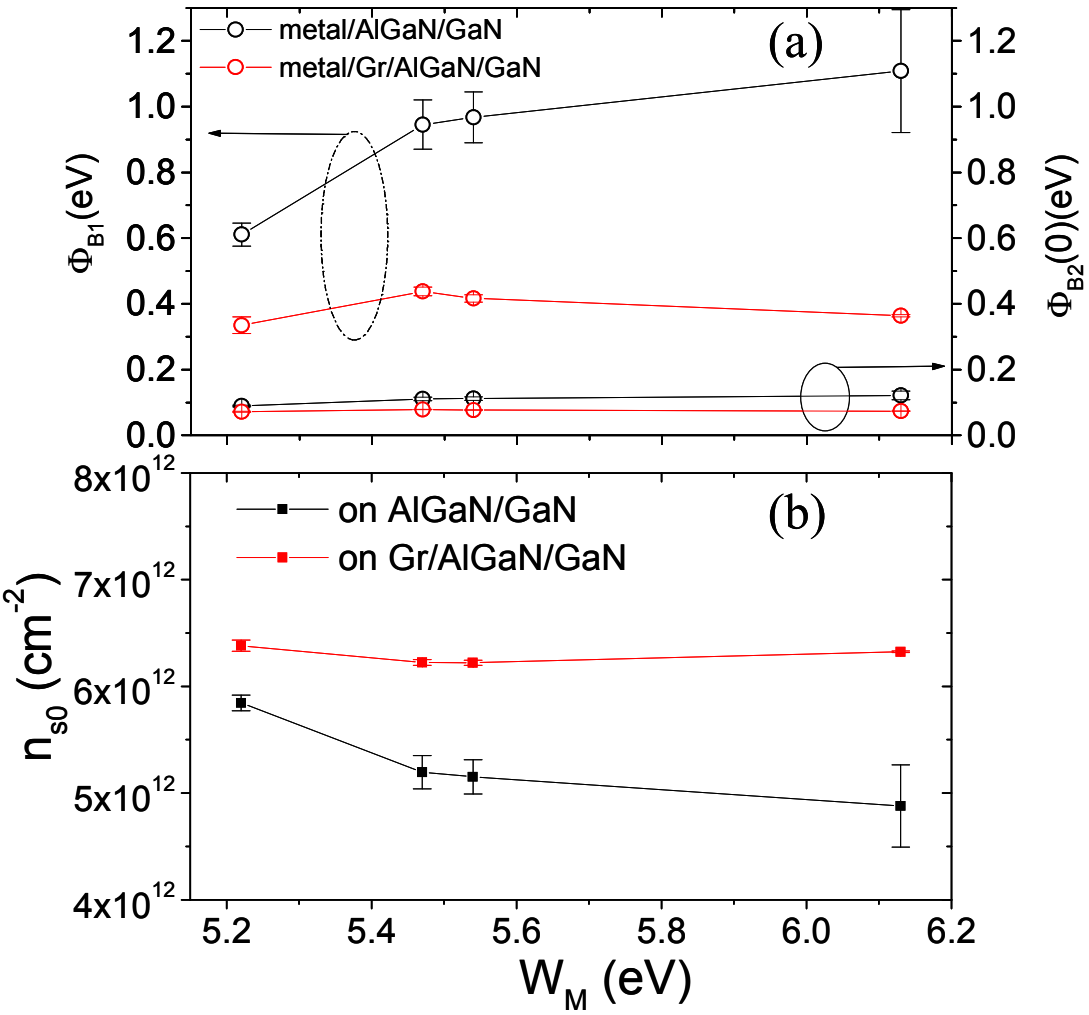


**Fig.4.** Behaviour of $\Phi_{B1}$, $\Phi_{B2}(0)$ (a) and $n_{s0}$ (b) vs the metal workfunction for the AlGaN/GaN and Gr/AlGaN/GaN heterostructures.

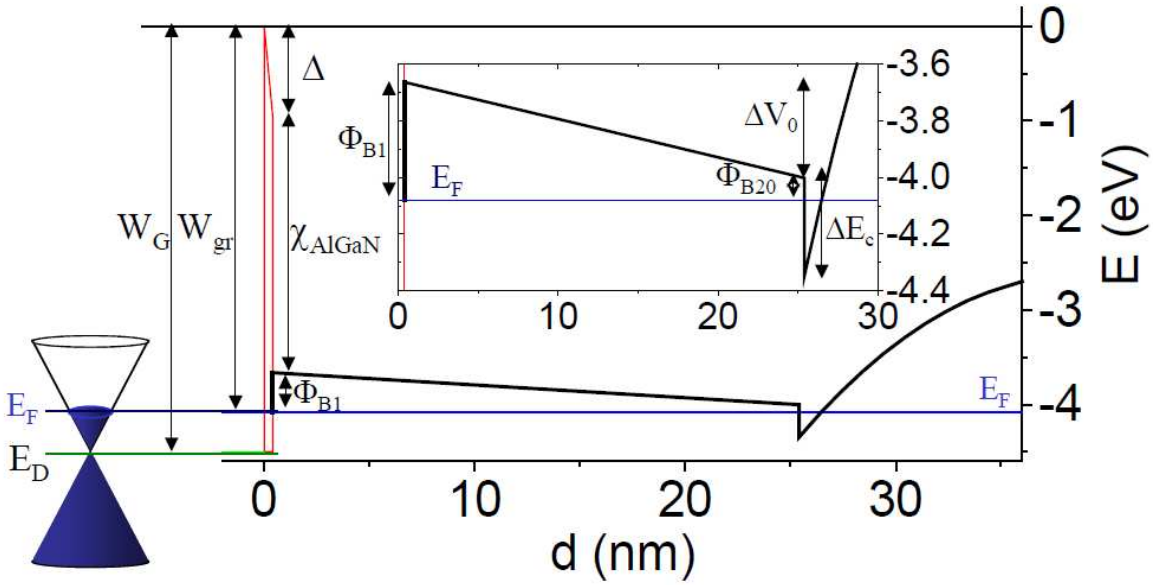


**Fig.5.** Calculated conduction band diagram for the Gr/AlGaN/GaN heterostructure at zero bias.

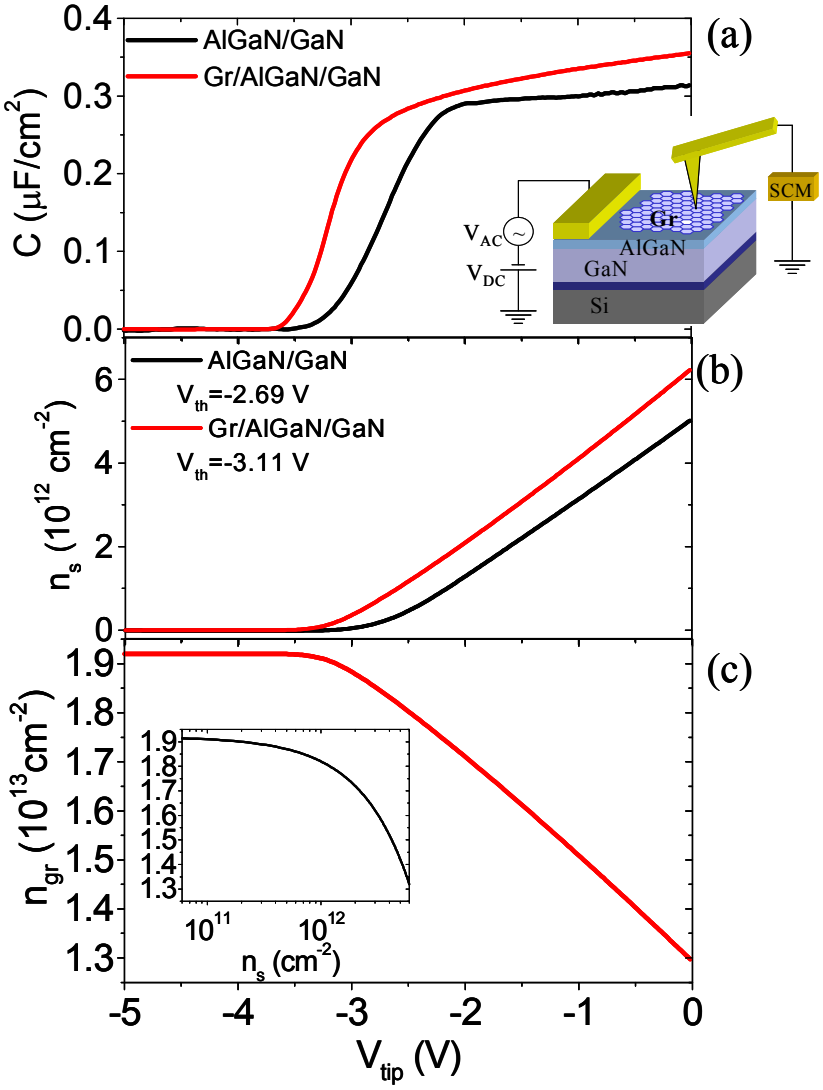


**Fig.6.** Two representative C-V curves (a) measured on the AlGaN/GaN and on the Gr/AlGaN/GaN heterostructures using an Au coated tip. In the insert, schematic representation of the SCM experimental setup. (b) Electron density $n_s$ of AlGaN/GaN 2DEG as a function of $V_{tip}$ obtained by integration of the representative C-$V_{tip}$ curves in (a). (c) Electron density $n_{gr}$ in graphene as a function of $V_{tip}$. The relation between $n_s$ and $n_{gr}$ is reported in the insert.